Hydrogeochemical and Isotopic Approach to Groundwater Management in a Mediterranean City Dependent on External Water Supply (Aix-en-Provence, SE France)

Christelle Claude, Hélène Miche, Ghislain Gassier, Ferhat Cherigui, Yves Dutour

water

MDPI

Article

Hydrogeochemical and Isotopic Approach to Groundwater Management in a Mediterranean City Dependent on External Water Supply (Aix-en-Provence, SE France)

Christelle Claude [1,*], Hélène Miche [1], Ghislain Gassier [1], Ferhat Cherigui [1] and Yves Dutour [2]

[1] CEREGE UM34, Aix Marseille University, CNRS, IRD, INRAE, Coll France, Technopôle de l'Environnement Arbois-Méditerranée, Avenue Louis Philibert, BP 80, 13545 Aix-en-Provence, France; miche@cerege.fr (H.M.); gassier@cerege.fr (G.G.); ferhat.cherigui@etu.univ-amu.fr (F.C.)

[2] Muséum d'Histoire Naturelles, 166 Avenue Jean Monnet, Parc Saint-Mitre, 13090 Aix-en-Provence, France; dutoury@mairie-aixenprovence.fr

* Correspondence: claude@cerege.fr

Abstract: Drought frequency and severity intensify with climate change, challenging many Mediterranean cities to face securing sustainable water supplies. In this context, groundwater emerges as a key but often overlooked resource, particularly in urban areas historically reliant on external drinking water systems. This study provides a comprehensive hydrogeological characterisation of the groundwater system in Aix-en-Provence (southeastern France), with a specific focus on hypothermal springs and the cold springs of the Vallon des Pinchinats, which historically supplied the town before the creation of the Canal de Provence by the company of the same name (Société du Canal de Provence (SCP)). By combining chemical and isotopic analyses ($\delta^{18}O$, $\delta^{2}H$, and chloride concentrations) with a statistical clustering (DACMAD method), we characterise the origin and dynamics of distinct water sources and evaluate their influence with surface water and external supply systems. Four key hydrological entities influencing the study area were identified. (1) regional precipitation (RRW) contributing significantly to groundwater recharge in the region. The isotope composition of the RRW was calculated ($\delta^{18}O$: −6.68‰, $\delta^{2}H$: −41.80‰, Cl: 2.2 mg/L) (2) Groundwater from the Oligocene aquifer (OG) characterised by an enrichment in chloride and sulphate. (3) Groundwater from the Cretaceous–Jurassic aquifer (CJG), a karstified aquifer from the Sainte-Victoire-Concors massif, which supplies the cold and hypothermal springs in Aix-en-Provence and multiple springs in the region. (4) Canal de Provence water (CPW) as an external water source, used for domestic supply, which has left a traceable signal in the local hydrosystem. The study reveals that cold springs of the Vallon des Pinchinats result from the mixing of Oligocene and Cretaceous–Jurassic groundwaters. Hypothermal springs (20–30 °C) circulate at moderate depths (165–500 m), unlike previous models suggesting deeper infiltration and mixing processes. This study contributes a novel hydrogeochemical and isotopic framework applicable to other Mediterranean urban areas facing similar pressures and highlights the strategic role that local groundwater can play in building long-term water resilience.

Keywords: hydro-chemistry stable isotopes; groundwater management; Mediterranean karstic aquifer; Oligocene aquifer; Cretaceous–Jurassic aquifer; Canal de Provence; clustering method; Aix-en-Provence (Fr)

Academic Editor: Nerantzis Kazakis

Received: 4 April 2025
Revised: 21 May 2025
Accepted: 23 May 2025
Published: 28 May 2025

Citation: Claude, C.; Miche, H.; Gassier, G.; Cherigui, F.; Dutour, Y. Hydrogeochemical and Isotopic Approach to Groundwater Management in a Mediterranean City Dependent on External Water Supply (Aix-en-Provence, SE France). *Water* **2025**, *17*, 1634. https://doi.org/10.3390/w17111634

1. Introduction

Since antiquity, Mediterranean cities have progressively adapted their water usage to meet the needs of expanding populations. Today, many urban centres in southern Europe continue to face the challenge of securing reliable drinking water supplies in the context of rapid demographic growth and increasing pressure on local resources. In several Mediterranean countries—including Algeria, Egypt, France, Israel, Italy, Spain, and Tunisia—a trend has emerged: moving away from local water sources, often considered overexploited or insufficient, toward more distant, abundant, and seemingly more sustainable supplies.

This strategy is not new. It mirrors the practices of ancient civilisations such as the Romans, who built extensive aqueduct systems to transport high-quality water over long distances, ensuring both urban development and public health. A notable example lies in Lower Provence, a region historically characterised by limited river systems and summer water shortages. In the second century AD, the Roman aqueduct of Traconnade supplied the city of Aquae Sextiae Salluviorum (modern Aix-en-Provence) with water from a spring located approximately fifty kilometres to the north, delivering around 0.2 m^3/s [1]. Today, this ancient solution is echoed by the Canal de Provence, which conveys water from the Verdon River over nearly 100 km to Aix-en-Provence, supplying around 5 m^3/s [2].

However, the current context of water management is increasingly shaped by the rising frequency and severity of droughts driven by climate change—even in regions traditionally considered water-resilient, such as Provence [3]. For example, Météo-France reported that July 2022 was the driest month since 1959, and the April–July 2022 period was the second driest on record, surpassed only by 1976. During this time, reservoirs such as the Lake of Sainte-Croix—one of the main water sources for the Canal de Provence—experienced drastic drops in water levels. These developments are prompting local and regional policymakers to reconsider water security strategies, including renewed attention to alternative and historically used local water sources [4].

Yet, in many areas, detailed knowledge about these local resources has been lost, due both to urban development and to the abandonment and lack of monitoring of springs and aquifers once used before large-scale inter-basin transfers [5]. Understanding the current quality, availability, and recharge dynamics of these local waters has, thus, become essential.

This study provides a novel contribution to the understanding of groundwater systems in Mediterranean environments by focusing on Aix-en-Provence—a medium-sized town in southeastern France that has received little attention in recent hydrogeological research. We analysed the chemical and isotopic compositions ($\delta^{18}O$ and $\delta^{2}H$) of both cold and hypothermal springs that historically supplied the city, allowing us to establish a contemporary hydrogeochemical profile and propose new interpretations regarding the origin and flow paths of these waters. While such isotopic and hydrochemical approaches are well documented in the broader Mediterranean region (for a synthesis, see [6]), they remain scarce in the French Mediterranean context [7–12].

By applying a multidisciplinary methodology that combines geochemistry, isotope hydrology, and new data-driven analysis (e.g., clustering), this research fills a significant regional knowledge gap. Beyond its local relevance, it offers a framework applicable to other Mediterranean urban areas facing increasing challenges in securing sustainable water supplies in the era of climate-induced droughts.

2. Study Area

2.1. Historical Context of Water Management in Aix-en-Provence

The Roman city of Aquae Sextiae Salluviorum, now known as Aix-en-Provence, was founded in 122 BC by the Roman consul Caius Sextius Calvinus. Its name is derived from

its founder and the thermal springs in the area. As the oldest Roman foundation in Gaul, Aix-en-Provence evolved from a fortified castellum to a thriving Roman city, supported by a network of aqueducts. Excavations conducted over the past three decades have provided valuable insights into the city's historical development [13–15].

Situated to the east of the Sainte-Victoire massif and its foothills (Figure 1), the city was strategically established on a mid-slope location, benefiting from thermal springs and a groundwater-rich subsoil.

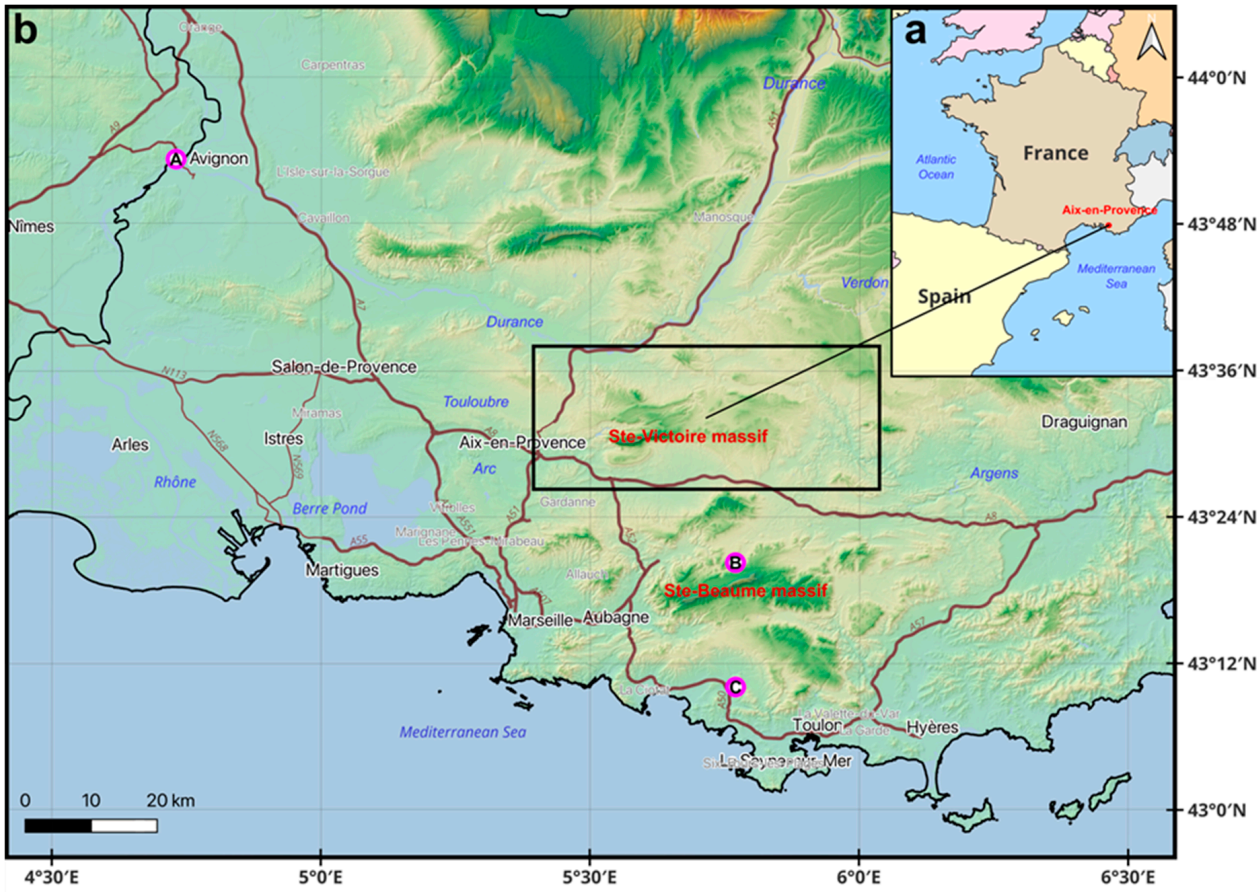

Figure 1. (**a**) General location of the study area around Aix-en-Provence (France) on a topographic map (scale 1:20,000,000; Lambert Conformal Conic Projection). (**b**) World Topographic Map (scale 1:650,000), highlighting the study area (829 km^2; 42.5 × 19.5 km) within a black rectangle. The locations of the three regional rainfall collection stations are also shown: A (Avignon), B (Beguines), and C (Castellet-Le Cas), corresponding to samples 30–32 in Table 1.

Shallow wells historically tapped into these resources, meeting the water needs of the early inhabitants. However, as urbanisation accelerated in the 1st century AD and public baths emerged by the end of the century, the demand for water exceeded local supplies, necessitating the construction of long-distance aqueducts. Two or possibly three aqueducts were built: the Vauvenargues and Saint-Antonin aqueducts (both potentially from the east), and the Traconnade aqueduct from the northeast. The Traconnade aqueduct was the most significant, transporting water from a major karstic spring more than 31 km north of Aix-en-Provence (Jouques, Bouches-du-Rhône) to supply the city.

By the late Middle Ages, local communities had developed water systems close to natural watercourses, though remote areas lacked water infrastructure. The Pinchinats district of Aix-en-Provence served as a long-standing water reserve, with a spring discharging drinkable water at an average rate of 30 L per second, first mentioned in 1185. Initially powering mills and irrigating gardens, this water source contributed to the city's

development, including the growth of the wool industry in the 15th century. Between 1854 and 1875, Aix-en-Provence was primarily supplied by the Zola Canal, which drew water from the Zola Dam on the Cause River, fed by the Vauvenargues Valley. Starting in 1875, with the construction of the Verdon Canal, the Zola Canal was gradually abandoned, and Aix-en-Provence began to receive its water supply from the Verdon. Since the early 1960s, the management and distribution of Verdon water to Aix-en-Provence has been handled by the Société du Canal de Provence.

Table 1. Sampling data for 32 water samples, including springs, stream waters, Canal de Provence water, and subsurface water collected from Aix-en-Provence (AeP) and the Sainte-Victoire Massif. A total of 26 water samples were collected in this study and compared with three samples from the literature (a: [16,17]). Additionally, three rainwater samples were included: A: Avignon (b: [18,19]), B: Beguines AMU station, and C: Castellet-Le Cas AMU station (c: [20]). The colour codes for the 'Sample type' category is consistent across all figures.

N°	Sample Name	Date	Sector	Sample Type	Latitude	Longitude	Z (Water) m	T °C	pH	X µS/cm
1	La_Foux_Meyrargues (Rock gallery)	1 April 2022	Ste-Victoire Massif North	Cold Spring Ste Victoire Massif	43.642003	5.54339722	213.7	15.3	7.25	618
2	Touloubre	1 April 2022	Aix-North	Stream water	43.577939	5.448397	296.1	9.1	7.76	927
3	Romegas	4 April 2022	Aix-North	Subsurface water	43.573408	5.448886	300.1	10.5	7.82	1620
4	Provence channel	4 April 2022	Aix-North	Canal de Provence water	43.573408	5.448886	299.1	10.8	8.11	419
5	Chateau de la Gaude (Hotel)	1 April 2022	Pinchinats	Cold Spring North AeP	43.569100	5.478831	355.7	13.2	7.60	506
6	Parraud	14 March 2022	Pinchinats	Cold Spring North AeP	43.555981	5.463069	289.0	14.6	7.20	938
7	Pinchinat 1 spring	14 March 2022	Pinchinats	Cold Spring North AeP	43.555922	5.469822	290.0	13.7	7.86	773
8	Fontlebre	14 March 2022	Pinchinats	Cold Spring North AeP	43.553736	5.457006	290.2	13.5	7.51	1274
9	Pinchinat 1	14 March 2022	Pinchinats	Stream water	43.551861	5.464261	263.1	10.6	7.89	762
10	Pinchinat 2	14 March 2022	Pinchinats	Stream water	43.550914	5.463042	256.7	9.9	7.93	724
11	Pinchinat 2 spring	14 March 2022	Pinchinats	Cold Spring North AeP	43.549742	5.462461	251.8	13.6	7.38	1012
12	Drinkable St Eutrope	27 February 2023	St Eutrope	Canal de Provence water	43.538608	5.452777	241.0	9.7	8.10	422
13	Raw St Eutrope	27 February 2023	St Eutrope	Canal de Provence water	43.538338	5.452219	243.0	9.9	8.07	420
14	Pinchinat 3 spring	14 March 2022	Pinchinats	Cold Spring North AeP	43.538589	5.457381	211.1	12.7	7.65	1089
15	Pinchinat 4 spring	14 March 2022	Pinchinats	Cold Spring North AeP	43.538511	5.457594	205.1	12.9	7.36	1021
16	Pinchinat 3	14 March 2022	Pinchinats	Stream water	43.538489	5.457731	207.5	9.6	8.08	644
17	Lavoir grand-mere	14 March 2022	Baret	Cold Spring East AeP	43.530392	5.462022	187.3	18.7	7.37	860
18	Torse Baret couverte	14 March 2022	Baret	Cold Spring East AeP	43.528814	5.462589	185.0	15.3	7.39	868
19	Sextius	25 April 2022	Aix intra muros	Hypothermal Spring	43.529339	5.440111	188.7	28.0	8.53	546
20	Chaudronniers	25 April 2022	Aix intra muros	Hypothermal Spring	43.528822	5.448947	192.7	30.9	7.93	581
21	Tanneurs	25 April 2022	Aix intra muros	Hypothermal Spring	43.527881	5.446203	181.7	20.7	8.28	687
22	Grand puits	25 April 2022	Aix intra muros	Hypothermal Spring	43.527553	5.448381	185.8	23.0	8.20	587
23	Fontaine Moussue (Chaudronniers)	7 April 2022	Aix intra muros	Hypothermal Spring	43.526900	5.449892	188.7	26.5	8.31	576
24	Source d'Argens	6 March 2023	Ste-Victoire Massif SE	Cold Spring Ste Victoire Massif	43.504065	5.907138	276.0	15.5	7.34	702
25	Source d'Argens	6 February 2024	Ste-Victoire Massif SE	Cold Spring Ste Victoire Massif	43.504065	5.907138	276.0	15.1	7.05	662
26	Font Taillade	6 February 2024	Ste-Victoire Massif SE	Cold Spring Ste Victoire Massif	43.526667	5.946667	270.0	14.5	7.09	740
27	Roques-Hautes (a)	1999–2000	Ste-Victoire Massif South	Cold Spring Ste Victoire Massif	43.527020	5.548180	265	13.1	7.35	497
28	Lavoir grand-mere (a)	1999–2000	Baret	Cold Spring East AeP	43.530392	5.462022	187.3	15.2	7.03	906
29	Chaudronniers (a)	1999–2000	Aix intra muros	Hypothermal Spring	43.528822	5.448947	192.7	30.6	7.07	582
30	A: Avignon (b)	1978–1989 1997–1998	Avignon	Rainfall	43.949156	4.818001	34.0	15.1	5.20	36.4
31	B: Beguines (c)	2018–2021	Ste-Baume Massif North	Rainfall	43.336670	5.772780	682.0	13.6		
32	C: Castellet Le Cas (c)	2018–2021	Ste-Baume Massif South	Rainfall	43.185600	5.782060	103.0	14.3		

2.2. Geological and Hydrogeological Context

The Aix-en-Provence basin consists primarily of Miocene and Oligocene sedimentary deposits, extending from the Berre lagoon in the west to the Gardanne basin in the east. It belongs to the limestone domain of western Lower Provence [21].

The study area is traversed by an NNE–SSW fault system known as the Pinchinats or Aix faults [22,23], which separates two distinct geological units: Cretaceous–Jurassic formations to the east (Sainte-Victoire Massif) and Oligocene formations to the west (Figure 2). The former contains an important aquifer outcropping in the surroundings in the bois de Keyrie area and extending to the north until the Durance River and tens of kilometres to the east (Figure 2b,c). This fault system continues northward, connecting with the Durance fault (Figure 2a,b). There is also a minor superficial aquifer in recent alluvial and colluvial deposits, traditionally tapped by wells [23].

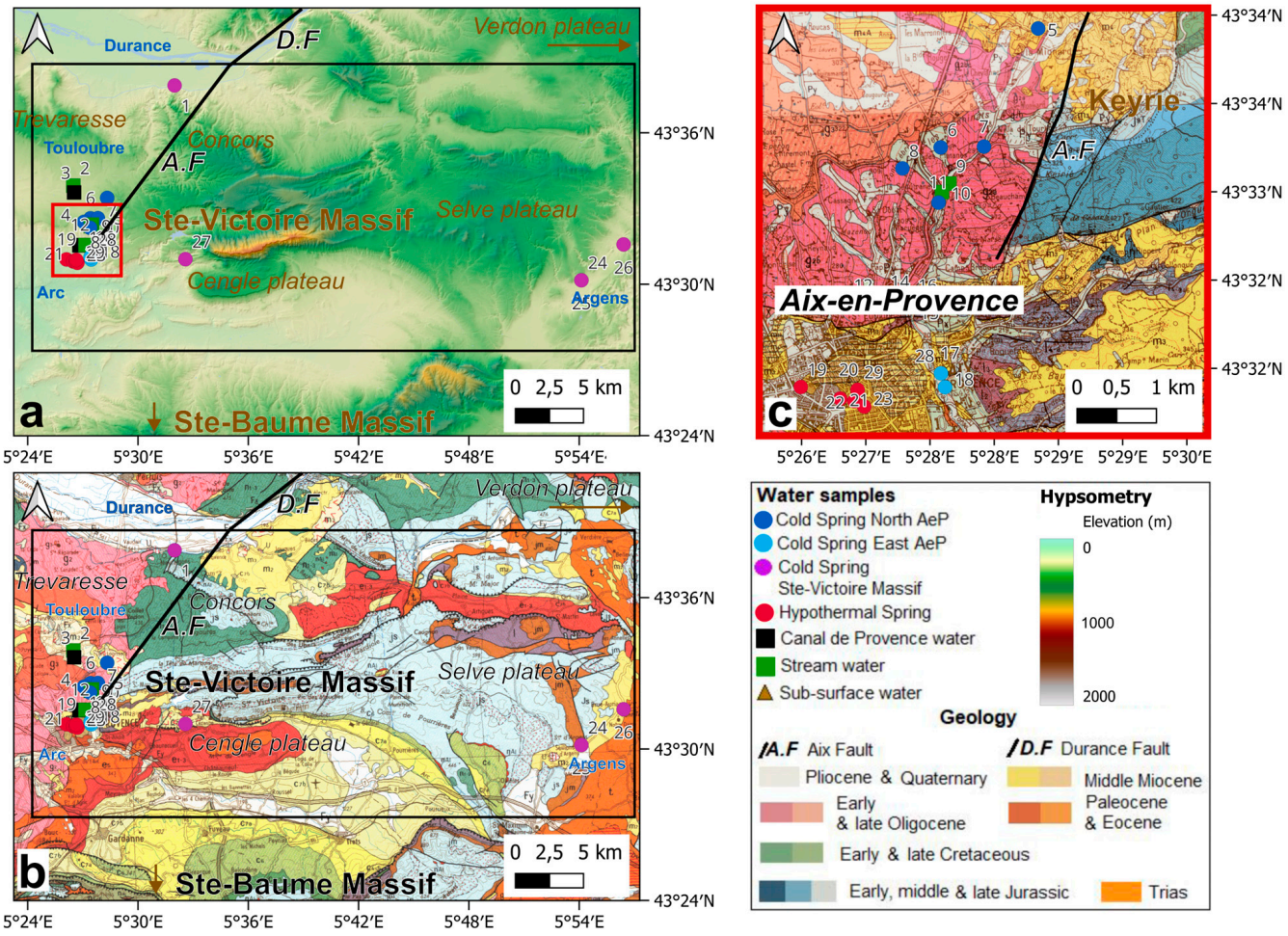

Figure 2. (**a**) Relief map of the study area (scale 1:350,000) showing the water sampling locations in Aix-en-Provence (AeP) and the Sainte-Victoire Massif. (**b**) Geological map of the study area (scale 1:250,000) with water sampling locations. (**c**) Detailed geological map of Aix-en-Provence (scale 1:60,000).

In Aix-en-Provence, thermal waters at 26 to 35 °C, with bicarbonate calcium and magnesium facies, emerge in various parts of the town centre in the form of ancient springs and from recent boreholes (Figure 2) [17]. In addition, several well-known cold springs exist in the surrounding area (Figure 2a,b). To the northwest, on the banks of the Durance River, the Sainte Victoire Massif discharges through the Meyrargues spring, at an elevation of 215 m, with an average flow rate of 700 m^3/h, and seasonal variations between 360 m^3/h during low water periods and 1350 m^3/h during floods. Further south, the La Foux spring is another significant water source. Northeast of Aix, the Vallon des Pinchinats area is home to several springs, including the Corneille (now inactive), Parraud, Tournon, and Vallon des Pinchinats springs. These springs are closely associated with fault systems or

artificial drainage galleries. The Meyrargues springs emerge along east–west faults within the karstic Sainte Victoire Jurassic aquifer, while la Foux and the Vallon des Pinchinats springs are thought to rise from the same Jurassic aquifer along the NNE–SSW-trending Aix-Pinchinats fault. It is generally accepted that water from the Jurassic karstified rises along the Pinchinats fault through the Oligocene formations [23] (Figure 2).

More to the east, the Argens and Font Taillade Springs flow out the Sainte Victoire Jurassic formation (Figure 2).

2.3. Climatic Context

Aix-en-Provence, located about 30 km inland, experiences a Mediterranean climate (Figure 1). The city's mean annual temperature is 15 °C, with average annual precipitation of 470 mm (Infoclimat, data series from 1975–2022). To contextualise this study's results, we compared them with isotopic data from nearby regions, specifically the GNIP station in Avignon to the northwest and the Sainte-Baume Massif stations southeast of the study area (Figure 1).

The Avignon GNIP station's long-term record (1997–2018) reports an average annual precipitation of 670 mm and a mean annual temperature of 15 °C (data from 2004–2014). The annual weighted $\delta^{18}O$ value of modern rainfall in Avignon is approximately −6‰ VSMOW, with more negative $\delta^{18}O$ values during the winter [18,19]. The Sainte-Baume Massif has a higher average annual precipitation of 900 mm and lower temperatures (around 10 °C), compared to Aix-en-Provence. Seasonal temperature and precipitation patterns are similar across the region, with peak temperatures in July and lows in January. Precipitation is distributed throughout the year, with two pronounced rainy seasons in spring and Autumn (September–December), during which approximately 80% of the annual rainfall occurs.

3. Materials and Methods

3.1. Sampling

The study area stretches from the town of Aix en Provence (AeP) in the east, to Meyrargues in the northeast (both in the Bouches du Rhône department), to the villages of Seillons and Brue Aurillac in the Var department.

Twenty-six water samples were collected from the study area between March 2022 and February 2024 (Figure 2) and reported together with six spring [16,17] and rain [18–20] results from the literature (Table 1).

The samples are categorised as follows: Thermal Spring water samples were taken in Aix-en-Provence intra muros (referred to as hypothermal waters #19, 20, 21, 22, 23, and 29). Further north, the Torse stream rises in the Vallon des Pinchinats. Several springs (referred to as cold springs North AeP, #5, 6, 7, 8, 11, 14, and 15) were collected, along with samples of the stream's water (referred to as stream waters #9, 10, and 16). Following the creek bed southwards, to the east of AeP intra muros lies the so-called "Baret sector". Here, small springs were sampled directly in the Torse bed (referred to as cold springs East AeP, #17, 18, and 28).

To the NW of Aix-en-Provence, a sample was collected in an artificial drainage gallery in the Oligocene formations of the Aix-en-Provence basin (referred to as subsurface water #3). The Toulouse, a small stream which rises to the west of the study area, was also sampled near this point (referred to as stream water #2).

Further north and east of the study area, spring waters from the Sainte Victoire limestone Massif were collected (referred to as Cold springs Ste Victoire, #1, 24, 25, 26, and 27).

SCP supplies the town with drinking water from the Bimont reservoir, fed by the Verdon River. We collected samples (referred to as Canal de Provence water) on a private

property (#4) but also directly at the treatment plant, before and after treatment (respectively, #13 and 12).

Finally, rain samples from the Avignon station [18,19] and two stations located in the Sainte Baume Massif (Castellet-Le Cas and Beguines AMU Stations) [20] are considered for comparisons.

3.2. Physico-Chemical Parameters and Alkalinity Titration

For each sample, temperature and electrical conductivity were measured using a WTW 340i conductivity meter (xylem Analytics, Weilheim, Germany). The pH and conductivity of the filtered water samples were determined with a WTW Multi-340i pH and conductivity meter (Table 1). Total alkalinity was measured by titration with 0.1 N hydrochloric acid (HCl) (Honeywell Fluka, Seelze, Germany), following the AFNOR standard NF T 90-036 [24]. At 20 °C, equivalence points for the CO_3^{2-}/HCO_3^- and HCO_3^-/H_2CO_3 buffering systems were determined at pH = 8.38 and pH = 4.44, respectively. The average reproducibility was approximately 5% based on samples replicates.

3.3. Cation and Anion Measurements by Capillary Electrophoresis and ICP-AES

Water samples for chemical analyses were collected in 50 mL plastic bottles (ref), using 0.45 µm cellulose acetate filters with water filter syringes.

Quantitative analyses of the major cations (Ca^{2+}, Mg^{2+}, Na^+, K^+, and NH_4^+) and anions (Br^-, Cl^-, SO_4^{2-}, NO_2^-, AND NO_3^--$H_2PO_4^-$) were determined by capillary electrophoresis (Agilent 7100) using a commercial eDAQ (Australia) C^4D detector [25] with a 50 um internal diameter, 50 cm long neutral capillary grafted with polyvinyl alcohol (PVA) with a background electrolyte composed of 2-(N-Morpholino)ethanesulfonicacid (MES), Histidine, and 18-crown-6 ether (Sigma-Aldrich, Saint-Louis, MO, USA) at pH = 6.0 (adapted from [26,27]). The multi-elemental solutions used for anion and cation calibration were prepared between the detection limit of each ion (~20 g/L) and 4.5 mg/L. Sampled water filtered at 0.45 um was diluted appropriately for measurement. The analytical reproducibility (1σ) was calculated from repeated measurements of multi-element control solutions. The average reproducibility was approximately 11% for Ca^{2+}, Mg^{2+}, NH_4^+, and Na^+, 15% for K^+, and around 9% for Cl^-, NO_3^-, SO_4^{2-}, and $H_2PO_4^-$.

These values are consistent with long-term reproducibility assessments, ranging from under 5% for Cl^-, SO_4^{2-}, Ca^{2+}, and Mg^{2+} to around 10% for NO_3^-, NO_2^-, Br^-, $H_2PO_4^-$, K^+, Na^+, and NH_4^+. Errors were estimated based on the measurement of three certified standard from NRC-Canada (Rain-12, Perade-17, Ontario-12) and control solutions of known composition. The standard error was approximately 9% for both cations and anions, consistent with external reproducibility. The ionic balance error was calculated to be less than 8% (Figure 3) for each analysed water sample (Figure 3).

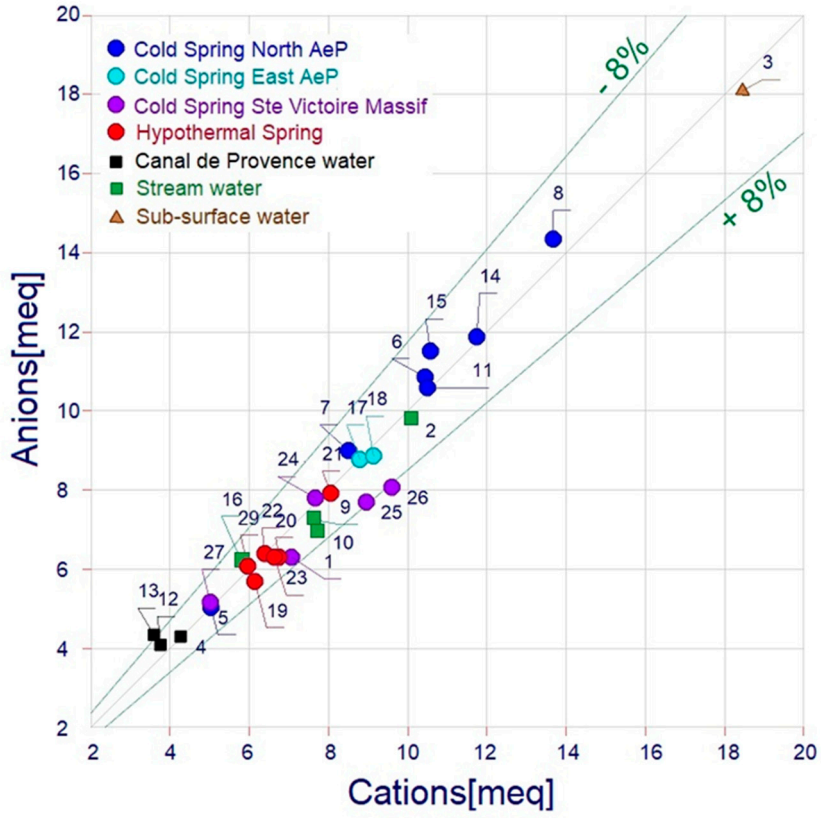

Figure 3. Sum of anions (meq/L) vs. sum of cations (meq/L) for hydrochemical data obtained by capillary electrophoresis and ICP-OES. The absolute uncertainty limit for ionic balance is 8%. Figure 3 was generated using the Diagrammes software v.9.20 [28].

3.4. Analysis of $\delta^{18}O$ and $\delta^{2}H$ Isotopes in Water Samples

Isotopic analysis samples were collected in 50 mL amber glass bottles, ensuring no air bubbles were present. Isotopic compositions of water samples were measured at CEREGE with a Picarro L2140i analyser (Picarro Inc., Santa Clara, CA, USA), equipped with a high-precision vaporiser and autosampler.

Isotope values are reported on the Vienna-Standard Mean Ocean Water (VSMOW) scale and the long-term precision is 0.023‰ for $\delta^{18}O$ and 0.078‰ for $\delta^{2}H$ [29].

3.5. Data Analysis Based on Clustering Method and Atypical Point Detection (Hereafter Referred to as the DACMAD Method)

This method relies on the iterative application of K-Means to perform clustering with dynamic atypical point detection. The process begins with the initialisation of clusters using four specific centroids representing different classes in the data.

At each iteration, valid points (non-excluded) are subjected to the K-Means algorithm, and the distances of each point to the centroid of its cluster are calculated. An adaptive threshold is defined based on the mean and standard deviation of these distances, allowing for the identification of atypical points, i.e., points that are too far from their cluster. This threshold characterises the maximum variance tolerated within the clusters and is determined by the prior setting of a variance factor. This factor reflects the variability allowed in the distribution of points within the clusters. A higher threshold allows for greater point dispersion, while a stricter threshold detects more atypical points. The points identified as atypical are then excluded, and the process is repeated until no new atypical points are detected. Once the atypical points are excluded, a final clustering is performed on the remaining points, and the data are assigned to clusters.

For visual representation purposes, the points are projected onto the first principal plane obtained through Principal Component Analysis (PCA). This allows for the visualisation of the main variability in the data in two dimensions, facilitating the graphical interpretation of clusters and atypical point. The method relies on mathematical principles of variance minimisation and distance-based clustering, making it robust in handling data anomalies and optimising cluster accuracy, as demonstrated in several studies on K-Means and outlier detection techniques [30–32].

4. Results

4.1. Physico-Chemical Parameters

The measurements of temperature, electrical conductivity (EC), and pH are summarised in Table 1. Based on temperature, the groundwaters can be distinguished into distinct groups (Figure 4):

- Cold springs: These exhibit temperatures between 10.5 °C and 18.7 °C;
- Hypothermal springs: characterised by higher temperatures, ranging from 20.7 °C to 30.9 °C;
- Surface waters: the Vallon des Pinchinats stream, Touloubre stream, and Canal de Provence waters characterised by the lowest temperatures, ranging from 9.1 °C to 10.6 °C.

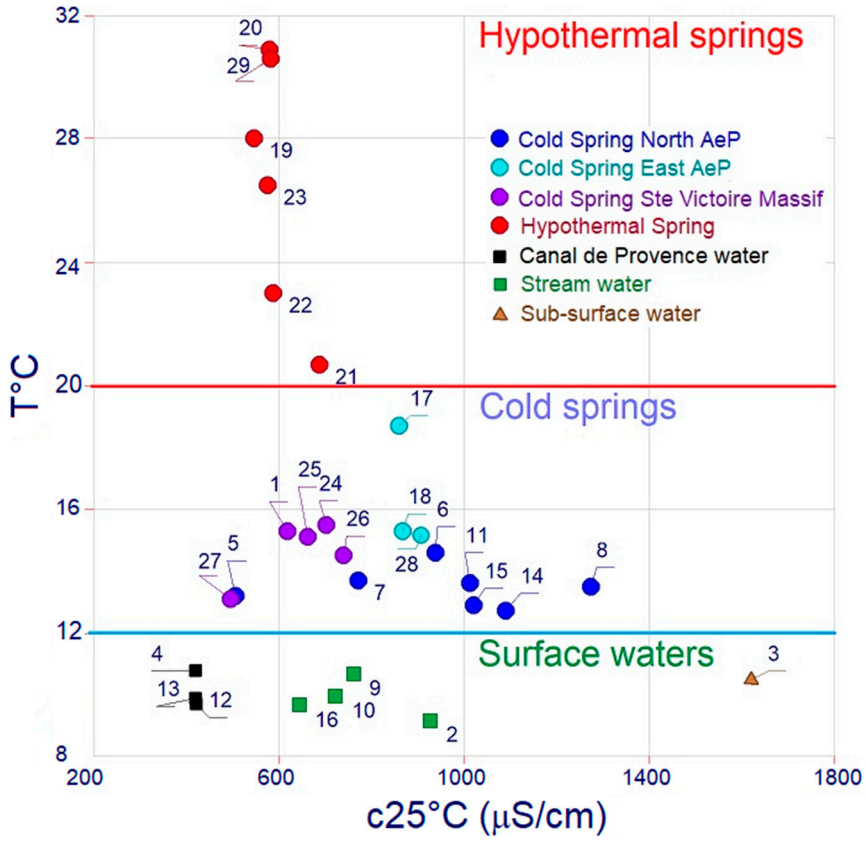

Figure 4. Classification of water samples based on electrical conductivity and temperature. Figure 4 was generated using the Diagrammes software v.9.20 [28].

The pH of cold springs waters remains below 8, consistent with typical regional waters. In contrast, hypothermal groundwaters exhibit slightly higher pH values, reaching up to 8.5. The Canal de Provence water samples also have a mildly alkaline pH of 8.1.

Regarding electrical conductivity, the Canal de Provence water samples present the lowest conductivity, at 400 µS/cm. The highest value is observed in the water collected

in the subsurface gallery excavated in sandy Oligocene formations (1620 µS/cm). Cold springs display a wide range from 500 to 1274 µS/cm: the springs from the Sainte Victoire massif plot at the lower hand of this range while the spring collected in the western branch of the Vallon des Pinchinat displays the highest conductivity. Springs from the Baret sector (cold springs East AeP) display intermediate values between the two. The hypothermal springs maintain a consistent EC around 600 µS/cm.

4.2. Water Chemistry

Analyses of anions and cations are reported in Table 2.

Table 2. Hydrochemical data for major and trace ionic species, as well as silica concentrations (mg/L) for 32 water samples, including the estimated chemical composition of rainwater in Aix-en-Provence [pH = 6.28; X = 25 µS/cm]. This estimation was obtained by analysing cumulative rainfall collected between July and December 2022 in Berre-l'Etang (23 km southwest of AeP, within the Arc River watershed, which flows south of the Sainte-Victoire Massif and through Aix-en-Provence). The colour codes for the 'Sample type' category is consistent across all figures.

	Hydrochemistry						**mg/L**					
N°	**Sample Type**	**Ca^{2+}**	**Mg^{2+}**	**Na^{+}**	**K^{+}**	**NH_4^{+}**	**HCO_3^{-}**	**Cl^{-}**	**SO_4^{2-}**	**$H_2PO_4^{-}$**	**NO_3^{-}**	**SiO_2**
1	Cold Spring Ste Victoire Massif	110	15.1	6.72	1.10	<LD	361	5.99	9.2	<LD	0.73	7.0
2	Stream water	112	24.0	52.7	8.12	1.50	310	86.2	103	0.95	4.18	8.8
3	Subsurface water	219	35.6	98.5	10.9	<LD	417	186	276	5.80	3.58	10.3
4	Canal de Provence water	61.7	5.1	16.7	1.59	<LD	176	26.3	27.5	1.79	2.51	4.5
5	Cold Spring North AeP	81.6	4.6	13.0	0.33	0.81	146	28.0	84.7	<LD	5.46	12.1
6	Cold Spring North AeP	167	15.5	17.9	1.59	<LD	476	36.6	78.5	0.91	22.8	11.2
7	Cold Spring North AeP	147	7.6	11.5	0.61	1.10	469	21.9	33.0	<LD	0.00	8.6
8	Cold Spring North AeP	144	46.4	58.4	4.49	<LD	405	126	197	2.68	0.00	23.5
9	Stream water	120	11.2	15.8	1.52	<LD	332	30.0	36.2	1.39	10.1	9.1
10	Stream water	122	10.9	15.9	1.49	<LD	315	31.7	37.2	1.42	3.75	8.8
11	Cold Spring North AeP	133	27.6	34.7	2.71	0.86	371	74.0	98.0	0.63	22.2	14.1
12	Canal de Provence water	50.0	6.0	15.9	2.67	<LD	179	22.0	23.1	<LD	3.25	3.7
13	Canal de Provence water	49.1	5.8	14.6	1.42	<LD	192	22.0	25.9	<LD	2.93	3.9
14	Cold Spring North AeP	158	25.9	36.1	3.66	1.20	395	82.6	140	0.63	8.90	13.7
15	Cold Spring North AeP	142	22.0	34.7	4.14	1.20	354	79.5	147	0.91	24.1	13.6
16	Stream water	75.8	12.6	21.1	2.22	<LD	237	38.9	49.4	1.62	8.05	8.0
17	Cold Spring East AeP	116	21.0	26.8	2.72	<LD	325	52.6	82.2	1.57	12.6	11.1
18	Cold Spring East AeP	125	18.8	28.8	1.90	<LD	320	56.6	83.5	1.57	14.6	10.7
19	Hypothermal Spring	73.1	19.2	19.1	2.45	<LD	250	25.1	38.8	<LD	4.71	8.8
20	Hypothermal Spring	79.4	24.4	16.5	2.01	<LD	279	25.0	39.3	1.77	8.49	10.3
21	Hypothermal Spring	101	19.5	26.2	10.1	<LD	295	31.2	89.5	1.67	16.4	11.3
22	Hypothermal Spring	77.1	20.0	18.2	3.43	<LD	269	28.7	42.7	2.19	12.1	10.2
23	Hypothermal Spring	78.2	23.5	16.7	2.19	<LD	250	27.2	40.7	3.25	29.3	11.2
24	Cold Spring Ste Victoire Massif	127	12.8	5.70	0.50	<LD	440	6.70	12.9	1.90	4.50	5.7
25	Cold Spring Ste Victoire Massif	145	16.9	6.90	1.11	<LD	435	8.76	12.8	<LD	2.97	6.5
26	Cold Spring Ste Victoire Massif	162	13.4	8.80	1.31	0.42	415	19.4	27.1	<LD	10.3	7.9
27	Cold Spring Ste Victoire Massif (a)	75.2	9.20	11.1	0.90	n.d.	253	18.8	21.6	1.16	1.1	5.1
28	Cold Spring East AeP (a)	n.d.	n.d.	n.d.	n.d.	n.d.	n.d.	45.6	107	n.d.	20.5	n.d.
29	Hypothermal Spring (a)	69.2	22.4	13.8	1.90	n.d.	277	23.3	36.3	0.31	6.24	11.1
30	Rainfall (b)	1.03	0.12	0.71	0.22	0.25	0.79	1.32	2.26	n.d.	1.49	n.d.
31	Rainfall (c)	n.d.	n.d.	n.d.	n.d.	n.d.	n.d.	n.d.	n.d.	n.d.	n.d.	n.d.
32	Rainfall (c)	n.d.	n.d.	n.d.	n.d.	n.d.	n.d.	n.d.	n.d.	n.d.	n.d.	n.d.
33	Estimated AeP rainfall	1.29	0.16	1.25	0.06	0.48	1.09	2.23	1.01	<LD	3.63	<LD
	Uncertainty (%)	6	8	10	20	10	7	2	2	4	9	5
	LD (µg/L)	20	25	25	25	20	200	1	25	25	25	15

The most widely used graphical tool for classifying the chemical nature of groundwater is the Piper diagram [33,34] (Figure 5). It provides a clear and synthetic visualisation of natural water chemistry, especially groundwater, allowing easy comparison of multiple samples and identifying ion dominance, water types (e.g., calcium-bicarbonate, sodium-chloride) and mixing of waters. Plotted as percentage of milliequivalents (meq%), the left triangle represents the major cations (Ca^2, Mg^{2+}, Na^{+} + K^{+}), the right triangle represents the major anions. The points from both triangles are projected into a central diamond, which allows a visualisation of the overall hydrochemical facies and a detection of mixing processes.

- The sample collected in the artificial drainage gallery (#3) plots in the chloride-sulphate domain.
- Cold springs span from the calcium-magnesium bicarbonate to the chloride-sulphate domain.
- Hypothermal waters have compositions intermediate between these two domains.

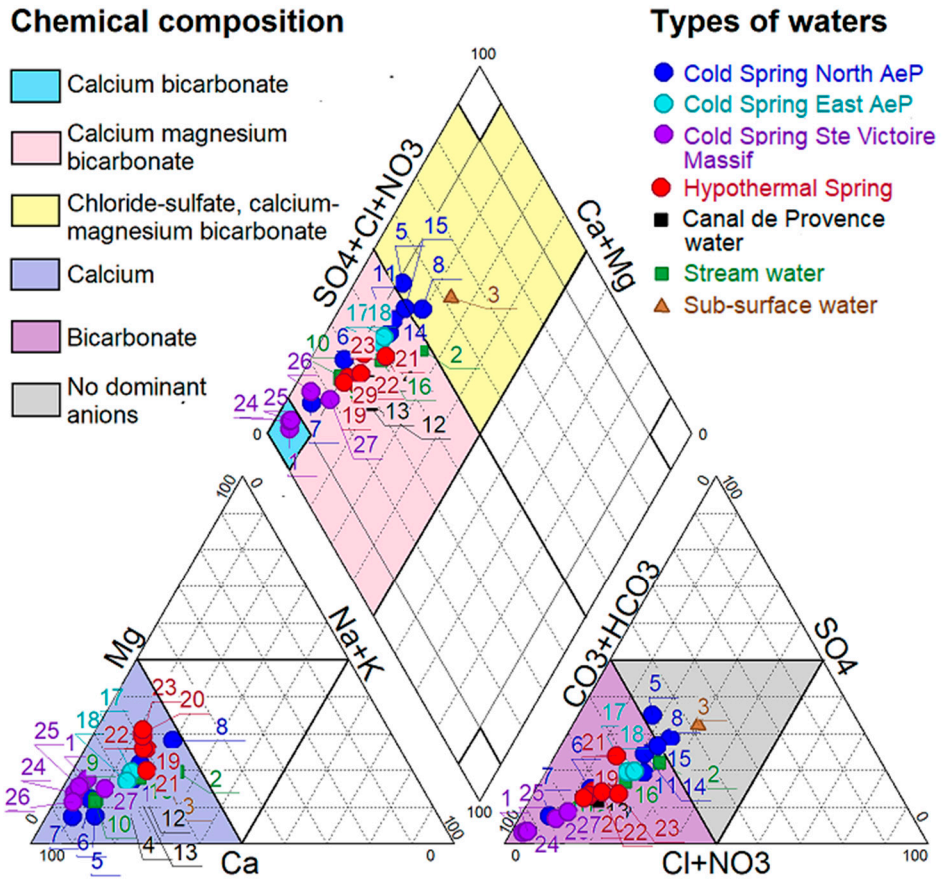

Figure 5. Piper diagram illustrating the geochemical composition of springs, stream waters, subsurface water, and Canal de Provence water (originating from the Verdon River). Figure 5 was generated using the Diagrammes software v.9.20 [28].

In summary, in terms of chemical composition two endmembers can be identified: the artificial drainage gallery water, enriched in chloride and sulphate, and the Sainte Victoire massif springs water dominated by bicarbonates and lower concentrations in sulphate and chloride (Figure 3).

4.3. Stable Isotopes

The oxygen ($\delta^{18}O$) and deuterium ($\delta^{2}H$) isotope compositions are provided in Table 3 and illustrated in Figure 6a.

Table 3. Stable isotope compositions ($\delta^{18}O$, $\delta^{2}H$) relative to VSMOW (‰) for the 32 water samples, including deuterium excess (d-excess = $\delta^{2}H - 8 \times \delta^{18}O$) and the calculated isotopic composition of estimated rainfall in Aix-en-Provence, assuming a chloride concentration (Cl^{-}) of 2.2 mg/L in precipitation (see Table 2). The colour codes for the 'Sample type' category is consistent across all figures.

Stable Isotopes		(V. VSMOW) ‰		
N°	Sample Type	$\delta^{18}O$	$\delta^{2}H$	d
1	Cold Spring Ste Victoire Massif	−7.48	−47.75	12.05
2	Stream water	−7.25	−49.22	8.82
3	Subsurface water	−7.55	−49.82	10.54
4	Canal de Provence water	−8.27	−56.95	9.25
5	Cold Spring North AeP	−6.88	−44.06	10.98
6	Cold Spring North AeP	−6.95	−44.83	10.75
7	Cold Spring North AeP	−6.82	−43.12	11.42
8	Cold Spring North AeP	−7.34	−48.93	9.79
9	Stream water	−6.76	−43.01	11.11
10	Stream water	−6.70	−42.68	10.91
11	Cold Spring North AeP	−7.12	−46.57	10.36

Table 3. *Cont.*

Stable Isotopes		(V. VSMOW) ‰		
N°	Sample Type	$\delta^{18}O$	$\delta^{2}H$	d
12	Canal de Provence water	−8.10	−55.92	8.87
13	Canal de Provence water	−8.11	−55.96	8.96
14	Cold Spring North AeP	−7.01	−45.55	10.49
15	Cold Spring North AeP	−7.30	−48.70	9.72
16	Stream water	−7.89	−53.42	9.71
17	Cold Spring East AeP	−7.51	−49.22	10.87
18	Cold Spring East AeP	−7.37	−48.22	10.77
19	Hypothermal Spring	−7.88	−51.40	11.61
20	Hypothermal Spring	−7.72	−49.59	12.16
21	Hypothermal Spring	−7.81	−51.20	11.29
22	Hypothermal Spring	−7.79	−50.56	11.76
23	Hypothermal Spring	−7.74	−49.51	12.37
24	Cold Spring Ste Victoire Massif	−7.02	−43.12	13.04
25	Cold Spring Ste Victoire Massif	−7.08	−44.40	12.25
26	Cold Spring Ste Victoire Massif	−6.73	−42.28	11.56
27	Cold Spring Ste Victoire Massif (a)	−7.80	n.d.	n.d.
28	Cold Spring East AeP (a)	−7.40	n.d.	n.d.
29	Hypothermal Spring (a)	−7.80	n.d.	n.d.
30	Rainfall (b)	−6.21	−40.80	8.88
31	Rainfall (c)	−6.99	−42.00	13.92
32	Rainfall (c)	−5.94	−35.70	11.82
33	Estimated AeP rainfall	−6.68	−41.80	11.63

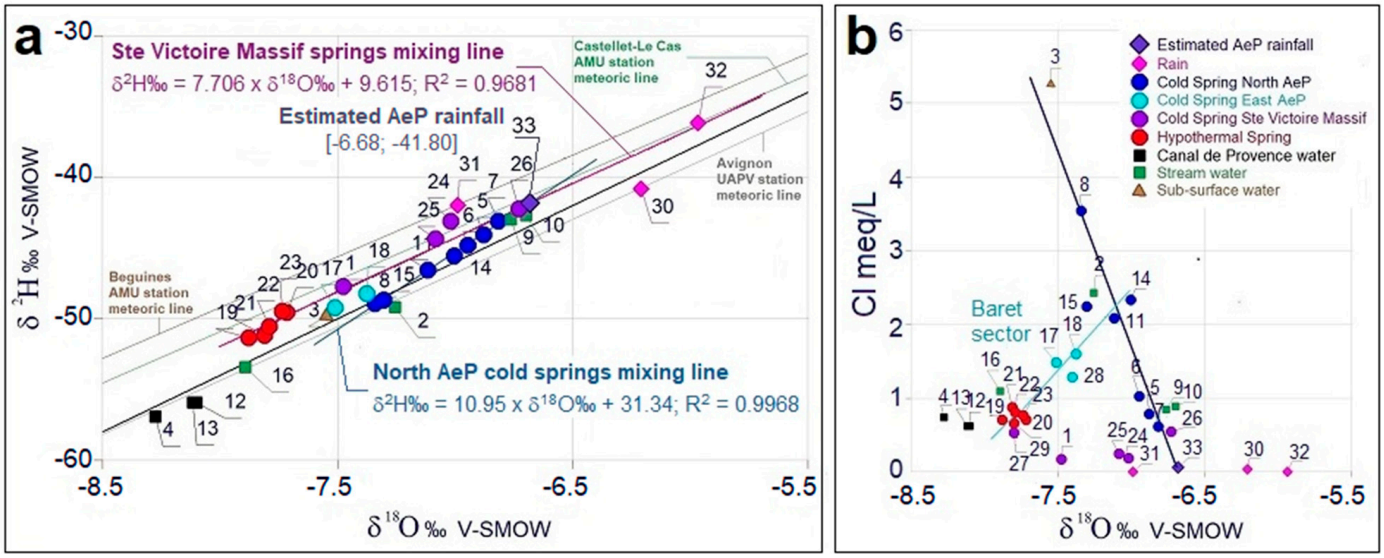

Figure 6. (**a**) Stable isotope data ($\delta^{18}O$, $\delta^{2}H$) relative to VSMOW (‰) plotted against the global meteoric water line (GMWL) [35] and three local meteoric water lines from weather stations surrounding the study area: Avignon GNIP station [20] and Beguines and Castellet-Le Cas (Aix-Marseille University, AMU) stations in the Sainte-Baume Massif [23]. The weighted average isotopic compositions of rainfall from the Avignon GNIP station (1997–2009; [36]) and the Castellet-Le Cas and Beguines stations (2019–2021) are also shown as solid pink diamonds (samples #30, 31, and 32 [20]). Cold springs from North Aix-en-Provence (samples #5, 6, 7, 8, 11, 14, and 15) align along a linear mixing trend ($y = 10.95x + 31.34$; $R^2 = 0.9968$), intersecting with the estimated local rainfall isotopic composition [$\delta^{18}O = -6.68$‰, $\delta^{2}H = -41.80$‰] (Table 3). Cold springs at the foothills of Sainte-Victoire (samples 1, 24, 25, and 26) together with the hypothermal springs (samples #19–23) follow a different regression line ($y = 7.706x + 9.615$; $R^2 = 0.9371$), intersecting with the weighted average isotopic composition of rainfall from Castellet-Le Cas (sample #32). (**b**) Chloride (meq/L) as a function of $\delta^{18}O$ V. VSMOW (‰). Two mixing lines have been highlighted: the first mixing line, in dark blue, originates from the estimated local rainfall at Aix-en-Provence (AeP) [Cl = 0.063 meq/L, $\delta^{18}O = -6.68$ ‰] (Tables 2 and 3, (**a**)) and concerns the cold springs north of AeP (5, 6, 7, 8, 11, 14, and 15). The second mixing line, in turquoise, passes through the points of the hypothermal springs, the cold springs East AeP in the Baret sector (#17, 18, and 28), and the cold springs in the Vallon des Pinchinats collected further to the north. Figure 6 was generated using the Diagrammes software v.9.20 [28].

Global meteoric line [35] and local meteoric water lines (LML) [18,20,36] from regions surrounding Aix-en-Provence, such as the northeast area and the Sainte Baume massif,

are included for comparison. Due to the absence of direct precipitation measurements for Aix-en-Provence, we used data from nearby stations to estimate the isotopic composition of local precipitation. These include Avignon, Castellet-Le Cas, and Beguines stations.

$\delta^{18}O$ and $\delta^{2}H$ values range from −8.27‰ to −6.70‰ and −55.96‰ to −42.68‰, respectively. Cold springs in the Vallon des Pinchinats (cold springs North AeP) exhibit the most enriched isotopic compositions, while the Provence Canal de Provence samples are the most depleted. Unlike their chemical compositions, isotopic values of hypothermal springs do not show intermediate values between the Oligocene (samples #3 and #1) and Cretaceous–Jurassic aquifer endmember (samples #24-25-26).

Stable isotopes of oxygen and hydrogen ($\delta^{18}O$ and $\delta^{2}H$) and chloride ions are conservative tracers used in hydrology to track the movement of water without undergoing chemical or biological changes during transport. Samples that line up on straight lines when projected in 2D or 3D diagrams with these tracers as X, Y, and Z coordinates can be used to highlight mixtures between two types of water and to characterise these mixing poles. These lines are called mixing lines. In Figure 6a, the cold spring samples align along a mixing line between two endmembers whose compositions need to be determined, possibly local precipitation and a deeper aquifer. The characterisation of these two poles will be dealt with in the discussion section. Hypothermal springs align together with the Sainte Victoire Massif springs along a line very close to the Castellet-Le Cas meteoric water line.

To assess mixing processes more precisely, we plotted chloride content against $\delta^{18}O$ (Figure 6b), showing that all samples lie between four endmembers:

- High chloride content and intermediate isotopic composition (dominant in samples #3, 8, and 2 collected in the Oligocene formation of Aix-en-Provence);
- Low chloride content, depleted isotopic composition endmember (cold springs Sainte Victoire massif);
- Regional precipitation endmember, enriched isotopic compositions and low chloride content;
- Low chloride content, most depleted isotopic composition endmember (Canal de Provence samples).

Cold springs in Vallon des Pinchinats (cold spring North AeP) and stream waters align between the high chloride content and intermediate isotopic endmember and regional precipitation, with one stream water sample influenced by the Canal de Provence (#16). Hypothermal springs and Canal de Provence waters, on the other hand, demonstrate rather uniform, depleted isotopic values, distinct from each other and from the cold springs from the Sainte Victoire Massif springs. Stream waters from the Baret sector (cold springs East AeP) exhibit intermediate isotopic characteristics between hypothermal and cold springs and surface waters in Vallon des Pinchinats. Roquehaute spring (#27) is isotopically depleted and enriched in chloride compared with the other Sainte-Victoire Massif samples.

Recharge altitudes, calculated from isotopic data [37], reveal that North AeP cold springs recharge at approximately 240 ± 50 m, while hypothermal springs have significantly higher recharge altitudes (480 ± 100 m). Canal de Provence water from Verdon River has the highest calculated recharge altitude (620 ± 120 m] (Figure 7).

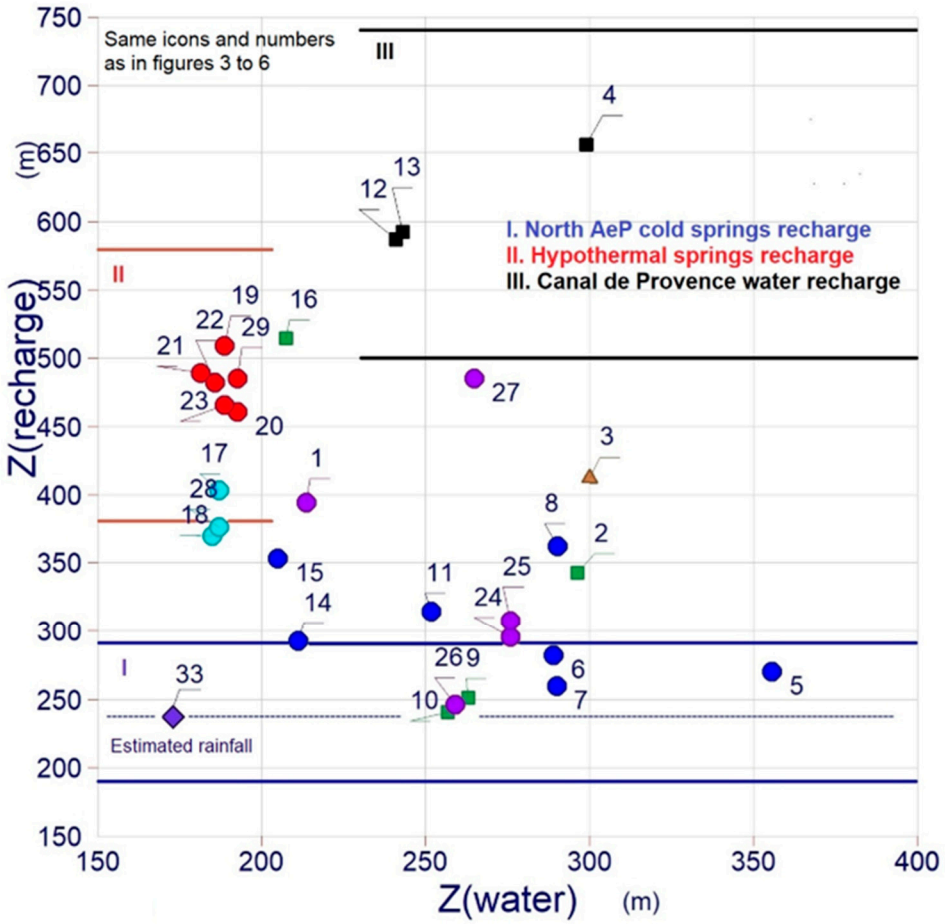

Figure 7. Calculated recharge altitudes based on $\delta^{18}O$ (after [37]). Three spring recharge zones are highlighted for the Aix-en-Provence hydrogeological system: North AeP [240 ± 50 m] and hypothermal [480 ± 100 m] springs recharge altitudes and Canal de Provence water recharge altitude [620 ± 120 m]. The composition of the estimated rain in Aix-en-Provence (#33) is used to calculate the North AeP springs recharge altitude. North AeP and hypothermal springs recharge zones are fed by the regional rainfalls (RRW). The samples plotting in between these three recharge zones are reflecting a mixture between the different hydrological entities: regional rainfall (RRW), groundwater from the Oligocene formations of Aix-en-Provence (OG), groundwater from the Cretaceous–Jurassic aquifer of the Concors-Sainte Victoire geological massif (CJG), and water from the Canal de Provence (CPW). Same symbols as in Figure 2. Figure 7 was generated using the Diagrammes software v.9.20 [28].

4.4. Clustering Method and Atypical Point Detection

Initially, we used the k means method (without excluding outliers). Because the threshold value was not controlled, the clusters formed were not consistent in terms of hydrogeology. To control this variance, in this study, we developed a DACMAD algorithm [38] (Python 3.12.0, packaged by conda-forge (main, October 3, 2023, 08:43:22) [GCC 12.3.0] on linux) used to highlight the hydrological entities (endmembers) present in the system as well as the mixtures between them. To do this, only fully conservative water body data were used (Cl, $\delta^{18}O$, and $\delta^{2}H$).

At the same time, the formation of the clustering classification is based on the designation of the initial centroids and the number of clusters. We tested a number of clusters ranging from 3 to 5.

Five samples are atypical points: Samples #31, 32, and 33 (rainfall from the Castellet and Beguines and Avignon stations, respectively), which are very far apart on axis 1, are clearly outside the game, naturally rejected by the DACMAD method. Samples #3 and to a lesser extent #8 are far apart on axis 2. All the other samples fall within a cluster: Cluster

1 includes samples #5, 6, 7, 9, 10, 24, 25, and 26. Cluster 2 includes samples #2, 11, 14, 15, 17, and 18. Cluster 3 includes samples #19, 20, 21, 22, 23, and 1. Finally, cluster 4 contains samples #4, 12, 13, and 16. The results are presented in a principal component analysis (PCA) plan defining axes 1 (Cl) and 2 ($\delta^{18}O$ and $\delta^{2}H$). Axes 1 and 2 carry 52% and 28% of the information, respectively (Figure 8). The PCA explains 80% of the variance in the total cloud.

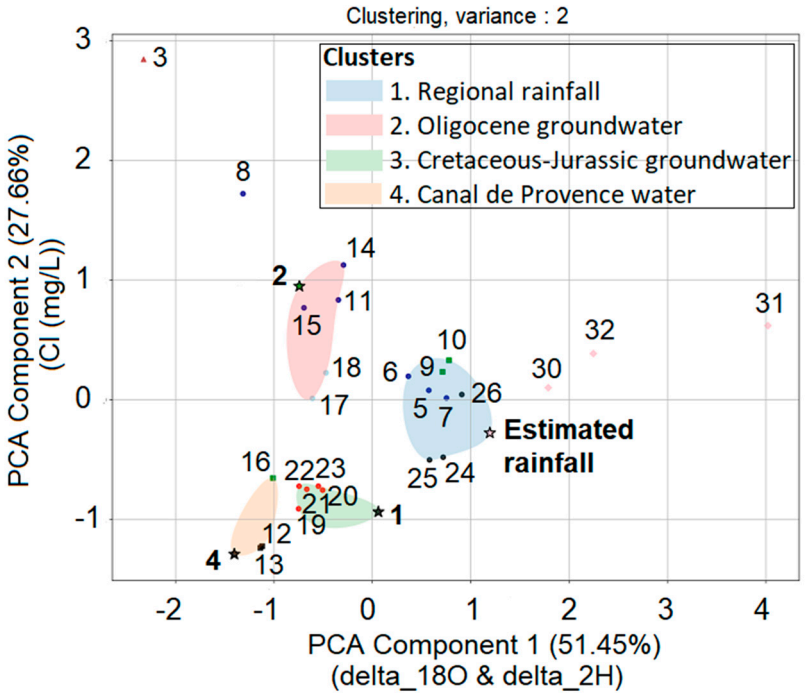

Figure 8. The DACMAD method [38] was used to highlight the hydrological entities (endmembers) present in the system and to a lesser extent the mixtures between them. The DACMAD results are showing four clusters obtained with points #33, 2, 1, and 4 as centroids for the entities RRW (cluster 1), OG (cluster 2), CJG (cluster 3), and CPW (cluster 4), respectively. The results are shown on the first principal plane obtained through Principal Component Analysis (PCA), which retains approximately 80% of the total inertia. Only fully conservative water body data were used (Cl, $\delta^{18}O$, and $\delta^{2}H$). The stars are the initial centroids. Same symbols as in Figure 2.

This DACMAD treatment shows that four clusters are very consistent with the number of hydrological entities involved in the study area: cluster 1, regional rainfall; cluster 2, groundwaters from the Oligocene sandy formations (Oligocene aquifer); cluster 3, groundwaters from the Concors-Sainte-Victoire massif (Cretaceous–Jurassic aquifer); and cluster 4, water from the Canal de Provence. The initial centroid of the cluster is chosen as a sample, thought to be representative of its hydrological entity.

Note that all the water samples from the Canal de Provence are in the same cluster (cluster 4). Similarly, all the hypothermal springs samples are in the cluster 3. On the other hand, samples of the "cold spring North AeP" are split within clusters 1 and 2. Similarly, stream water samples do not belong to one cluster but are distributed between three clusters (1, 2, and 4).

5. Discussion

The study of groundwater in Aix-en-Provence revealed distinct physico-chemical and isotopic characteristics among water sources. Cold springs, hypothermal springs, and surface waters were differentiated by temperature, pH, and EC, with hypothermal springs showing higher temperatures and slightly more alkaline pH. Chemical analysis using Piper diagrams identified two compositional endmembers: chloride-sulphate-rich

waters and bicarbonate-dominated Sainte Victoire springs. Stable isotope data ($\delta^{18}O$, $\delta^{2}H$) and chloride content further distinguished water sources and revealed mixing trends among up to four endmembers. Recharge altitudes derived from isotopes ranged from ~240 m for cold springs, higher altitudes for the hypothermal springs, and to over 600 m for the Canal de Provence water. A clustering analysis using the DACMAD algorithm effectively highlighted four endmember compositions (regional rainfall, groundwaters from the Sainte Victoire massif, Oligocene aquifer, and the Canal de Provence water) and water mixing processes.

The chemical and isotopic results described above indicate that it is not straightforward to determine the respective influences or mixing processes of these four entities within the study area, as well as the underground circulation patterns. As a first step, we will attempt to define each of these entities based on their chemical and isotopic characteristics. We will then estimate their relative influence on the cold and hypothermal spring waters of Aix-en-Provence, before proposing a conceptual circulation model.

5.1. Characterisation of the Hydrological Entities in the Study Area

5.1.1. Regional Rainfall (RRW)

To accurately characterise the composition of rainfall as an aquifer recharge source, a long-term dataset spanning several years is necessary. Unfortunately, precipitation in the Aix-en-Provence area could not be collected during this study. However, a series of rainwater samples was collected 23 km southwest of Aix-en-Provence (Berre-l'Étang) over a specified period (Figure 1a), and their chemical composition was analysed. To estimate the isotopic composition of the recharge, we relied on long-term datasets from regional monitoring stations, such as Avignon to the northwest [18,35] and the Sainte-Baume massif to the southeast of the study area [20] (Figure 1a).

As shown in Figure 6a,b, none of the literature data appear to correspond to the composition of rainfall recharging the cold and hypothermal springs of Aix-en-Provence. Moreover, the DACMAD method confirms that these data points are atypical points, plotting outside all clusters. Therefore, we estimated the chloride and isotopic composition of the regional rainfall. First, we assumed that the composition of regional rainfall should fall on the regression line titled "Sainte Victoire Massif Mixing Line" in the $\delta^{18}O$ vs. $\delta^{2}H$ diagram. This regression line has a slope of 7.7, very close to the slope of global meteoric water lines, particularly that of Castellet-Le Cas (southern Sainte-Baume Massif). Second, we assumed that the regional rainfall composition should fall on the regression line for "Cold Spring North AeP Mixing Line". We then calculated the intersection of these two regression lines, representing it in Figure 6a,b (diamond) and reporting it in Tables 2 and 3 (sample #33: $\delta^{18}O$: −6.68‰, $\delta^{2}H$: −41.80‰, Cl: 2.2 mg/L). We believe this composition is representative of rainfall in the Aix-en-Provence region, making it one of the four key entities in the hydrogeological system (Regional Rain endmember). This composition was used to define the initial centroid of this entity using the DACMAD method (Figure 8).

5.1.2. Characterisation of the Hydrological Entity "Groundwater from the Oligocene Formations of Aix-en-Provence (OG)"

We collected and analysed three samples that can be considered representative of the chemical and isotopic composition of the OG hydrological entity, particularly marked by an enrichment in sulphate and chloride ions (Figure 5, Table 2). These are sample #2 (surface water from the Touloubre stream), #3 (subsurface water from an artificial drainage gallery), and #8 (cold spring water from North AeP). Samples #2 and 8 are very similar in terms of oxygen and hydrogen isotope compositions but different in terms of chloride and sulphate ions. Sample #3 (Romegas), characterised by the highest chloride and sulphate contents, is more isotopically depleted.

To determine which of these samples is the most representative of the "OG" entity, we applied the DACMAD method. In this approach, initial centroids are assumed to be representative of the hydrological entities. Defining the centroids of each cluster is crucial, and we based our selection on the chemical and isotopic compositions of all collected samples, supplemented by literature data. Initially, we tested points #33, 8, 1, and 4 as centroids for the entities RRW, OG, CJG, and CPW, respectively.

Variance is another key parameter in determining which and how many points belong to a cluster. Additionally, we conducted a sensitivity analysis on the threshold value. This threshold, multiplied by the standard deviation of distances within the cluster, defines the maximum variability allowed within clusters. A threshold of 2 implies dispersion equal to twice the standard deviation of the data distribution. Our sensitivity tests indicated that from a value of 2 onwards, cluster composition stabilises in accordance with hydrogeological knowledge (initial centroids). Furthermore, an interval extending two standard deviations above and below the mean contains approximately 95% of the data, assuming a normal distribution. This confidence interval (2σ) is a standard measure in geochemistry.

The clustering results, represented in PCA plots 1 and 2, show that the initial centroids fall outside the clusters, particularly point #8 (OG), point #33 (RR), and point #1 (CJG). This implies the need to redefine the initial centroids. Among the three samples that could potentially represent the OG entity, only point #2 (Touloubre River) is included in a cluster. Thus, we tested this point as the initial centroid for the OG hydrological entity. The analysis yielded four clusters, each incorporating its initial centroid. This suggests that modifying only the initial centroid of one cluster resolves the issue of centroid misalignment in the other clusters. Finally, the Touloubre River sample is representative of the "Oligocene Aquifer" entity, suggesting that in this area, Touloubre River waters are partially recharged by the Oligocene sandy formations of Aix-en-Provence. In the same area, the Font Lèbre spring (sample #8), located in the northwestern branch of the Vallon des Pinchinats, situated in Oligocene terrains, is according to the literature recharged by the deep karstified Jurassic aquifer [23]. The result we obtained using the DACMAD method, which indicates that point #8 is an atypical point, does not seem to strongly support the hypothesis of [23]. Sample #3 (Romegas) appears to be even more atypical than point #8. We propose that this results from the infiltration of water within a subsurface gallery excavated in sandy Oligocene formations, which are enriched in chlorides and sulphates. Consequently, the observed chemical composition of sample #3 is likely influenced by localised hydrogeochemical processes.

5.1.3. Present-Day Influence of Canal de Provence Waters in the Hydrogeological System of Aix-en-Provence

Point #16, which shows chemical and isotopic characteristics partially influenced by waters from the Canal de Provence, is incorporated into cluster 4 together with the Canal de Provence samples (Figures 6 and 8). Surface waters in the Vallon des Pinchinats appear to be influenced by SCP water, especially near the St. Eutrope station. These results suggest a minor but noticeable contribution of SCP water to the hydrogeological system of Aix-en-Provence, likely through surface water infiltration or sewage system contributions. This influence is detectable despite the hypothermal origin of many of the springs in the area.

5.2. Origin of the Cold Spring Waters in the Vallon des Pinchinats

The stable isotopes of oxygen ($\delta^{18}O$) and deuterium (δ2H), along with chloride concentrations, serve as conservative tracers in hydrology to identify mixing processes between different water entities.

In the Vallon des Pinchinats, cold springs and stream samples exhibit linear trends in both $\delta^{18}O$-δ2H and Cl-$\delta^{18}O$ relationships, suggesting binary mixing between two end-

members: one characterised by high chloride and low δ^{18}O-δ2H values and the other by low chloride and high δ^{18}O-δ2H values (herein referred to as the "North AeP cold springs mixing line") (Figure 6a,b).

As said above, the high chloride and low δ^{18}O-δ2H values endmember characterises the OG hydrological entity, which is more likely represented by the Touloubre river sample in the vicinity of Aix-en-Provence. The high δ^{18}O-δ2H, low-chloride endmember dominates the cold spring samples from the northeastern branch of the Vallon des Pinchinats (samples #5, 6, and 7). Previous hydrogeological studies indicate that these springs may be fed by the karstic Jurassic aquifer of the Sainte-Victoire-Concors complex, via the NNE–SSW fracture network along its eastern boundary [23]. This Jurassic aquifer is the most significant in the region, feeding other springs along its northern (Meyrargues and La Foux), northeastern (Traconnade), and eastern (Argens) boundaries. However, isotopic and chloride data from La Foux, Traconnade, and Argens springs, measured in this study, do not align with the Pinchinat mixing line (Figures 2 and 6a,b). These samples plot above the Pinchinat mixing line in the δ^{18}O-δ2H diagram, indicating a distinct D-excess and more depleted δ^{18}O values for given chloride contents. This suggests that the Jurassic karstic aquifer alone cannot account for the recharge of the Vallon des Pinchinats cold springs, requiring the contribution of a less depleted δ^{18}O water source.

The results of the DACMAD method also show that the cold springs from North AeP are distributed between two clusters, consistent with subsurface mixing in the Vallon des Pinchinats between two hydrological entities: cluster 2 is supposed to be representative of the OG entity and cluster 1 is supposed to be representative of the RRW entity, as point #33, selected as the centroid of cluster 1, is well-positioned within the cluster, which suggests a significant influence of RRW in the cold springs from North AeP. The contribution of regional precipitation is less depleted in δ^{18}O and δ2H, and therefore, it is likely to significantly contribute to the Vallon des Pinchinats hydrological system.

In summary, the isotopic and chemical compositions of the cold springs in the Vallon des Pinchinats can be explained by a mixture of two distinct water sources: the western branch of the valley, dominated by chloride-sulphate-type groundwaters, and the eastern branch, a mixture of regional precipitation and groundwaters from the Cretaceous–Jurassic.

5.3. Origin of the Hypothermal Spring Waters in Aix-en-Provence and Circulation Pattern

The isotopic composition of hypothermal waters in Aix-en-Provence shows small variations, and aligns with cold springs such as La Foux, Traconnade, and, to a lesser extent, Argens. These cold springs, along with the regional precipitation plot along the local meteoric water line from Castellet, imply a shared recharge origin. Importantly, hypothermal spring samples belong to the cluster 3 (Figure 8) supposed to be representative of groundwaters from the Concors-Sainte-Victoire massif (Cretaceous–Jurassic aquifer), indicating a genetic link to this formation.

Previous studies indicate that these cold springs likely emerge from the karstic Cretaceous–Jurassic aquifer system associated with the Sainte-Victoire and Concors massifs, extending eastward [16,17,23]. Our findings support a similar recharge source for the hypothermal groundwater of Aix-en-Provence, with the more isotopically depleted waters reflecting a recharge from higher altitudes (400–500 m), such as in the Concors-Sainte-Victoire massif (Figure 7).

The elevated temperatures characteristic of these hypothermal waters suggests deeper groundwater circulation compared to the cold springs in the Vallon des Pinchinats. In the absence of significant thermal anomalies (e.g., deep-seated volcanism), the depth of groundwater circulation can be estimated using the regional geothermal gradient (approximately 30 °C/km) and the temperature difference between the surface (mean annual

temperature of 15 °C in Aix-en-Provence) and the measured hypothermal groundwater temperatures (ranging between 20 °C and 30 °C). This suggests circulation depths of 165 to 500 m. However, more precise measurements of the local geothermal gradient are necessary to confirm these estimates. The NNE–SSW fault system in Aix-Pinchinats, a network of parallel fractures, likely facilitates this deep circulation, though its full vertical extent is not well defined.

Two water samples, i.e., #17 and #18, (cold springs East AeP), given their location within the Torse watercourse, may have compositions that closely resemble those of the nearby surface water samples (#11, #14, and #15). Logically, they fall within cluster 3, along with those samples (Figure 8). In addition, samples #17 and #18 display the highest temperature among the cold spring waters from Aix-en-Provence (Table 1), which also suggests some contribution from hypothermal springs. The contribution of hypothermal water in these samples is also supported by their intermediate isotopic compositions, which fall between those of the hypothermal springs and the cold springs of the Vallon des Pinchinats (Figure 6a,b). Based on chloride concentrations, these waters appear to result from a 50–50% mixture of hypothermal and cold spring waters. If this mixing occurs near the surface with no significant heat exchange with the environment, the expected water temperature should range between 16.5 °C and 21.5 °C, consistent with the measured values of 15.3 °C and 18.7 °C. These findings suggest that hypothermal springs may discharge into surface streams, with mixing occurring close to the surface.

6. Conceptual Circulation Model and Implications for Water Resource Management

In part 5, through chemical and isotopic analyses ($\delta^{18}O$, δ2H, and chloride concentrations), combined with statistical clustering (DACMAD method), we have identified four key hydrological entities influencing the study area: (1) regional precipitation (RRW), (2) groundwater from the Oligocene aquifer (OG), (3) groundwater from the Cretaceous–Jurassic aquifer (CJG), and (4) the Canal de Provence water (CPW).

The study reveals a dual groundwater circulation system (Figure 9):

- Cold springs in the Vallon des Pinchinats result from the mixing of Oligocene groundwater and karstic Jurassic groundwater, with a strong recharge component from regional rainfalls. Their isotopic composition suggests relatively shallow circulation pathways with limited residence time.
- Hypothermal springs originate from deeper circulation within the Cretaceous–Jurassic aquifer, as indicated by their more depleted $\delta^{18}O$ and δ2H values and their elevated temperatures (20–30 °C). By applying a regional geothermal gradient (30 °C/km), we estimate that these waters circulate at depths between 165 and 500 m, where they undergo prolonged interaction with the surrounding rock matrix before resurfacing.
- Surface water–groundwater interactions are evident in the Torse-Baret sector, where mixed water samples display characteristics of both cold and hypothermal springs. This suggests active discharge zones where deeper flow systems converge into the subsurface waters.

The identification of the hypothermal water recharge zone in the Sainte-Victoire and Concors massifs is consistent with the results of previous studies [16,17]. However, our interpretation of the circulation pattern is different. They suggested that this recharge water infiltrates at a depth of 1000 m and reaches a temperature of 40 to 45 °C. The authors proposed to explain the lower temperatures observed in the hypothermal waters of Aix-en-Provence (26–34°) by a mixture of these hot waters with those of a local aquifer present at a depth of 150 m, the temperature of whose waters is between 17 and 22 °C. Firstly, no water with a temperature of 40 °C was sampled. Secondly, our results show that the chemical

and isotopic composition of the thermal waters of Aix-en-Provence is fairly homogeneous (Figure 6a,b). It is, therefore, not easy to demonstrate that the composition of these waters is the result of a mixture. From our point of view, it is, thus, simpler to consider a shallower infiltration depth (150–400 m). Hence, we have no evidence of the influence of a local underground reservoir (apart from the Oligocene formations) located at a depth of 150 m.

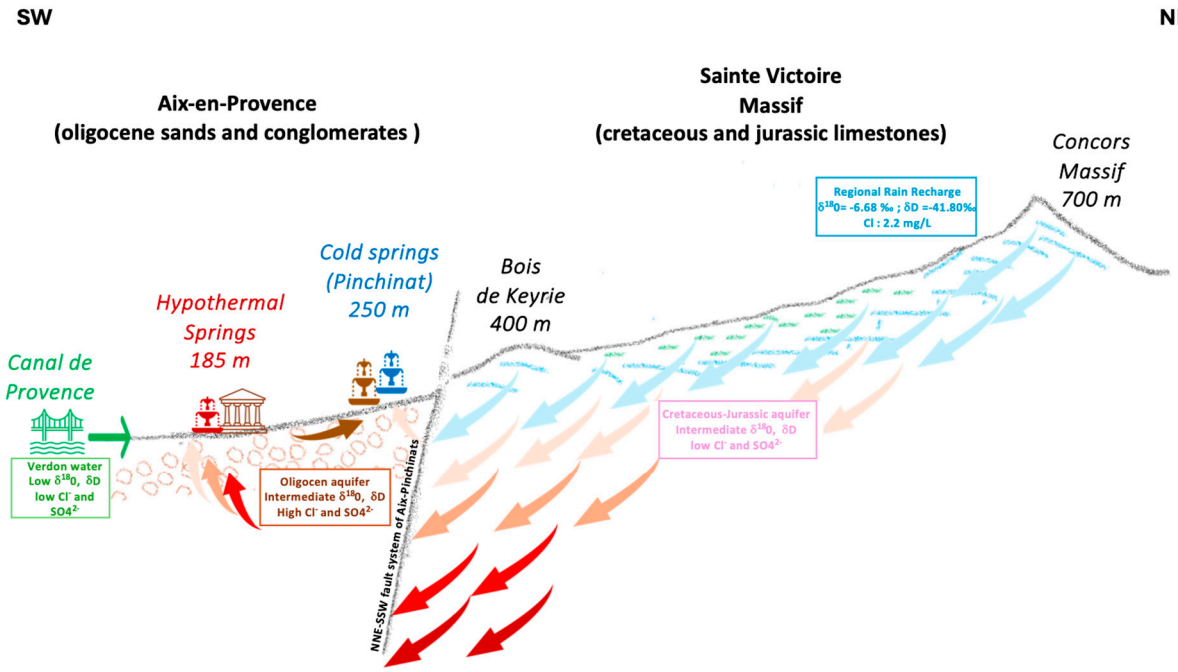

Figure 9. A conceptual circulation model is illustrated on a schematic geological cross-section-oriented SW–NE, extending from the Oligocene basin of Aix-en-Provence to the Concors area, within the Cretaceous–Jurassic formation of the Sainte-Victoire Massif. Recharge Process: precipitation infiltrates through fractured limestone formations in the Sainte-Victoire massif and surrounding areas, recharging the karstic Cretaceous–Jurassic aquifer (light blue arrows). A portion of the infiltrated water percolates through Oligocene formations (brown arrow), contributing to local groundwater storage and feeding shallow wells and rivers (e.g., Touloubre River). Groundwater Flow Pathways: shallow flow paths (50–150 m depth, in light blue) feed the cold springs, where groundwater mixes with infiltrated rainwater and Oligocene groundwater (in brown) before emerging in the Vallon des Pinchinats. Deep flow paths (>150 m depth) extend into the Cretaceous–Jurassic aquifer, where water circulates through karstified and faulted zones (orange and red arrows). This prolonged residence time at depth increases water temperature before it resurfaces as hypothermal springs (in red). Fault networks, particularly the NNE–SSW fault system of Aix-Pinchinats, play a crucial role in guiding groundwater circulation, facilitating upward migration of hypothermal water along fracture zones. Surface Water Influence and Anthropogenic Inputs: surface water from the Canal de Provence (in green) and nearby streams show minor interactions with the groundwater system, likely through leakage and artificial infiltration.

7. Conclusions

This study refines the understanding of the groundwater system in Aix-en-Provence by characterising the sources, flow paths, and mixing processes of both cold and hypothermal springs.

Through the integration of isotopic, chemical, and statistical methods, we identify a dual groundwater circulation system governed by karstic recharge from regional precipitation, with distinct contributions from the Oligocene and Cretaceous–Jurassic aquifers. Our findings support a more homogeneous and moderately deep circulation model for the hypothermal springs than previously assumed, and confirm that regional rainfall remains the primary recharge source.

The identification of distinct groundwater sources and their circulation patterns has important implications for urban water management:

- Potential for local groundwater as a strategic resource: The presence of clearly identified aquifer systems suggests that local springs—long sidelined in favour of external water transfers could provide a complementary water source, particularly during drought periods.
- Protection of recharge areas: The sustainability of infiltration zones for both cold and hypothermal springs depends on preserving karstic recharge areas in the Sainte-Victoire and Concors massifs. Land use and development policies must take into account this vulnerability.

Given the growing pressure on regional water resources together with the increasing frequency of droughts in Mediterranean regions, this research highlights the need for a re-evaluation of local groundwater as part of adaptive, diversified, and resilient water supply strategies. Further investigations, including tracer experiments and hydrogeochemical modelling, precise geothermal gradient measurements, and long-term monitoring of groundwater recharge, could provide additional insights into groundwater residence times and recharge dynamics, which will be essential to refine recharge estimates and guide long-term planning for the Mediterranean region.

Author Contributions: Methodology, C.C., H.M., G.G., F.C. and Y.D.; Formal analysis, H.M. and F.C.; Data curation, C.C. and H.M.; Writing—original draft, C.C., H.M. and G.G.; Writing—review & editing, C.C., H.M. and G.G.; Supervision, C.C.; Project administration, C.C.; Funding acquisition, C.C. All authors have read and agreed to the published version of the manuscript.

Funding: The project leading to this publication has received funding from Excellence Initiative of Aix-Marseille University—A*MIDEX, a French "Investissements d'Avenir" programme—Institute for Mediterranean Archaeology ARKAIA (AMX-19-IET-003).

Data Availability Statement: The original contributions presented in this study are included in the article. Further inquiries can be directed to the corresponding author.

Acknowledgments: This study was supported by the Aquedaix, Amorce-ARKAIA (Aix-Marseille Université) project. We would like to thank Christine Vallet-Coulomb and David Au Yang for their help with water stable isotopes (PANISS platform, CEREGE). We would also like to thank Jules Fleury (SIGEO platform, CEREGE), who used his DTM to specify our GPS coordinates and the altitude of our samples in Aix-en-Provence. We also thank Bernard Fino, Marc Fuhry, and Vincent Verdu for their help on the field. Finally, we would like to thank the staff of the Aix-en-Provence sewage work and the drinking water department, who helped us organise and carry out our sampling. Our warmest thanks also to Michael Wharton for proofreading the manuscript and correcting in British English and to Adrien Lenormand for his expertise with cartography and QGIS software Version 3.34 Prizren.

Conflicts of Interest: The authors declare no conflicts of interest.

References

1. Fino, B.; Fuhry, M. L'aqueduc romain d'Aix-en-Provence/Traconnade. *Rev. Archéol. De Narbonn.* **2020**, *53*, 101–146. [CrossRef]
2. Jean, M. *Les Architectes de l'eau en Provence, de la Renaissance au XXe Siècle*; Actes Sud: Arles, France, 2011; 544p.
3. Vinci, G.; Maddaloni, L.; Mancini, L.; Prencipe, S.A.; Ruggeri, M.; Tiradritti, M. The Health of the Water Planet: Challenges and Opportunities in the Mediterranean Area: An Overview. *Earth* **2021**, *2*, 894–919. [CrossRef]
4. Fragkou, M.C.; Vicent, T.; Gabarrell, X. An ecosystemic approach for assessing the urban water self-sufficiency potential: Lessons from the Mediterranean. *Urban. Water J.* **2016**, *13*, 663–675. [CrossRef]
5. Evsell, X. Urban Groundwater: Barcelona City Case Study. Ph.D. Thesis, Universitat Politècnica de Catalunya, Barcelona, Spain, 2011.
6. Al Haj, R.; Merheb, M.; Halwani, J.; Ouddane, B. Hydrogeochemical characteristics of groundwater in the Mediterranean region: A meta-analysis. *Phys. Chem. Earth* **2023**, *129*, 103351. [CrossRef]

7. De Montety, V.; Radakovitch, O.; Vallet-Coulomb, C.; Blavoux, B.; Hermitte, D.; Valles, V. Origin of groundwater salinity and hydrogeochemical processes in a confined coastal aquifer: Case of the Rhône delta (Southern France). *Appl. Geochem.* **2008**, *23*, 2337–2349. [CrossRef]
8. Charmoille, A.; Binet, S.; Bertrand, C.; Guglielmi, Y.; Mudry, J. Hydraulic interactions between fractures and bedding planes in a carbonate aquifer studied by means of experimentally induced water-table fluctuations (Coaraze experimental site, southeastern France). *Hydrogeol. J.* **2009**, *17*, 1607–1616. [CrossRef]
9. Gattacceca, J.C.; Vallet-Coulomb, C.; Mayer, A.; Claude, C.; Radakovitch, O.; Conchetto, E.; Hamelin, B. Isotopic and geochemical characterisation of salinization in the shallow aquifers of a reclaimed subsiding zone: The southern Venice Lagoon coastland. *J. Hydrol.* **2009**, *378*, 46–61. [CrossRef]
10. Bicalho, C.C.; Batiot-Guilhe, C.; Seidel, J.L.; Van-Exter, S.; Jourde, H. Investigation of groundwater dynamics in a mediterranean karst system by using multiple hydrogeochemical tracers. In *Advances in Research in Karst Media, Environmental Earth Sciences*; Andreo, B., Carrasco, F., Durán, J.J., LaMoreaux, J.W., Eds.; Springer: Berlin/Heidelberg, Germany, 2010; pp. 157–162. [CrossRef]
11. Maréchal, J.C.; Lachassagne, P.; Ladouche, B.; Dewandel, B.; Lanini, S.; Le Strat, P.; Petelet-Giraud, E. Structure and hydrogeochemical functioning of a sparkling natural mineral water system determined using a multidisciplinary approach: A case study from southern France. *Hydrogeol. J.* **2014**, *22*, 47–68. [CrossRef]
12. Santoni, S.; Huneau, F.; Garel, E.; Aquilina, L.; Vergnaud-Ayraud, V.; Labasque, T.; Celle-Jeanton, H. Strontium isotopes as tracers of water-rocks interactions, mixing processes and residence time indicator of groundwater within the granite-carbonate coastal aquifer of Bonifacio (Corsica, France). *Sci. Total Environ.* **2016**, *573*, 233–246. [CrossRef]
13. Mocci, F.; Nin, N. Aix-en-Provence, Pays d'Aix, Val de Durance. *Bull. Soc. Hist. Nat. Provence* **2006**, *52*, 11–27.
14. Leveau, P. Les aqueducs d'Aquae Sextiae et la gestion de l'eau sur le territoire de la cité. In *Aix-en-Provence Et Son Approvisionnement en Eau*; Nin, N., Ed.; Presses Universitaires de Provence: Aix-en-Provence, France, 2006; pp. 79–95.
15. Nin, N. *Aix en Archeologie—25 Ans de Decouvertes*; Revue Archéologique de Picardie; Snoeck: Gand, Belgium, 2014; 532p.
16. Cordoba, J. Ressource Hydrothermale du Bassin d'Aix-en-Provence. Master's Thesis, Neuchâtel University, Neuchâtel, Switzerland, 1999.
17. Vuataz, F.D.; Rossi, P.; Lettry, Y.; Tanguy, E. Compréhension et gestion du système hydrothermal d'Aix-en-Provence. *Hydrogeol. J.* **2003**, *11*, 250–265.
18. Celle, H.; Daniel, M.; Mudry, J.; Blavoux, B. Signal pluie et traçage par les isotopes stables en Méditerranée occidentale. Exemple de la région avignonnaise (Sud-Est de la France). *C. R. Acad. Sci. Ser. IIA-Earth Planet. Sci.* **2000**, *331*, 647–650. [CrossRef]
19. Celle-Jeanton, H.; Travi, Y.; Loÿe-Pilot, M.D.; Huneau, F.; Bertrand, G. Rainwater chemistry at a Mediterranean inland station (Avignon, France): Local contribution versus long-range supply. *Atmos. Res.* **2009**, *91*, 118–126. [CrossRef]
20. Garin, T.H. Recharge and Flow Structures in Carbonate Aquifers. Ph.D. Thesis, Aix-Marseille Université, Marseille, France, 2022.
21. Glintzboeckel, C.; Durozoy, G. *Étude des Ressources Hydrologiques Et Hydrogéologiques du Sud-Est*; BRGM Report; BRGM: Orléans, France, 1968.
22. Rousset, C. Hydrogéologie. Origine et venue au jour des eaux thermales d'Aix-en-Provence: État actuel de la question. *C. R. Hebd. Des Séances De L'acad. Des Sci.* **1972**, *274*, 1261–1264.
23. Silvestre, J.P.; Sedan, O. *Identification de Sites de Sondages de Recherche d'eau au Nord-Est d'Aix-en-Provence*; BRGM Report; BRGM: Orléans, France, 1988.
24. *NF T90-036*; Essais des Eaux—Détermination de L'alcalinité (Titre Alcalimétrique Et Titre Alcalimétrique Complet). AFNOR: Paris, France, 1977.
25. Kuban, P.; Hauser, P.C. 20th anniversary of axial capacitively coupled contactless conductivity detection in capillary electrophoresis. *Trends Anal. Chem.* **2018**, *102*, 311–321. [CrossRef]
26. Zemann, A.J. Capacitively coupled contactless conductivity detection in capillary electrophoresis. *Electrophoresis* **2003**, *24*, 2125–2137. [CrossRef]
27. Neaga, I.-O.; Iacob, B.C.; Bodoki, E. The analysis of small ions with physiological implications using capillary electrophoresis. *J. Liquid. Chromatogr. Relat. Technol.* **2014**, *37*, 2072–2090. [CrossRef]
28. Simler, R. Diagrammes Software, Version 9.20. Laboratoire d'Hydrogéologie: Avignon, France. Available online: https://terre-et-eau.univ-avignon.fr/logiciels (accessed on 16 April 2025).
29. Vallet-Coulomb, C.; Couapel, M.; Sonzogni, C. Improving memory effect correction for high-precision water isotope analysis. *Rapid Commun. Mass. Spectrom.* **2021**, *35*, e9108. [CrossRef] [PubMed]
30. Jain, A.K. Data clustering: 50 years beyond K-means. *Pattern Recognit. Lett.* **2010**, *31*, 651–666. [CrossRef]
31. Xu, R.; Wunsch, D.C. Survey of clustering algorithms. *IEEE Trans. Neural Netw.* **2005**, *16*, 645–678. [CrossRef]
32. Chawla, S.; Gionis, A. K-means: A unified approach to clustering and outlier detection. In Proceedings of the SIAM International Conference on Data Mining (SDM), Austin, TX, USA, 2–4 May 2013; pp. 189–197. [CrossRef]
33. Piper, A.M. A graphic procedure in the geochemical interpretation of water analyzes. *EOS Trans. Am. Geophys. Union* **1944**, *25*, 914–928. [CrossRef]

34. Cloutier, V.; Lefebvre, R.; Savard, M.M.; Bourque, É.; Therrien, R. Hydrogeochemistry and groundwater origin of the Basses-Laurentides sedimentary rock aquifer system, St. Lawrence Lowlands, Québec, Canada. *Hydrogeol. J.* **2006**, *14*, 573–590. [CrossRef]
35. Craig, H. Isotopic Variations in Meteoric Waters. *Science* **1961**, *133*, 1702–1703. [CrossRef] [PubMed]
36. Seraphin, P. Contribution of Isotopic Tracing to Hydrogeological Modeling of the Crau Aquifer. Ph.D. Thesis, Aix-Marseille Université, Marseille, France, 2016.
37. Guglielmi, Y.; Mudry, J.; Blavoux, B. Estimation of the water balance of alluvial aquifers in regions of high isotopic contrast: An example from southeastern France. *J. Hydrol.* **1998**, *210*, 106–115. [CrossRef]
38. Available online: https://gitlab.osupytheas.fr/ggassier/dacmad (accessed on 22 May 2025).